Computers and Structures 230 (2020) 106184

Contents lists available at ScienceDirect

Computers and Structures

journal homepage: www.elsevier.com/locate/compstruc

A quasi-static non-linear modal analysis procedure extending Rayleigh quotient stationarity for non-conservative dynamical systems

Nidish Narayanaa Balaji, Matthew R.W. Brake *

Department of Mechanical Engineering, Rice University, Houston, TX 77005, United States

ARTICLE INFO

Article history:
Received 9 October 2019
Accepted 9 December 2019

Keywords:
Nonlinear modal analysis
Hysteretic systems
Quasi-static modeling
Rayleigh quotient
Courant-Fischer theorem

ABSTRACT

Non-linear Modal Analysis (NMA) refers to a class of analysis procedures that seek to characterize non-linear dynamical systems similar to how classical linear modal analysis characterizes the natural frequencies and mode shapes of linear systems. The current study proposes an extension to the stationarity of Rayleigh quotients, a classical technique for linear modal analysis, for non-linear, non-conservative, dynamical systems. The approach, termed *Rayleigh Quotient-based Nonlinear Modal Analysis* (RQNMA), formalizes each mode as a finite non-trivial perturbation about a static solution that is locally stationary in the work done. Apart from offering a theoretical basis for the concept of non-linear modes, this circumvents several limitations in previous methods (for example, *Quasi-Static Modal Analysis* (QSMA)), such as inconsistencies in handling static forces, assumptions on mode-shape change, etc. As with other NMA procedures, RQNMA is formulated for the characterization of the amplitude-dependent natural frequency (stiffness) and damping ratio (dissipation) near/at the resonances. The estimated stiffness and dissipation characteristics are compared with modal backbones generated from frequency-domain approaches, which typically are computationally more expensive than the presented approach. Comparisons are conducted using different benchmark models, placing special emphasis on structures with pre-stressed frictional contacts, in order to bring out the strengths and shortcomings of the presented approach to contextualize its applicability.

© 2019 Elsevier Ltd. All rights reserved.

1. Introduction

Nonlinear modal analysis (NMA) was first developed to study conservative systems [8,19,35,37,44–46,52]. With recent theoretical advances that enable the study of non-conservative systems, NMA has become a useful technique for characterizing non-conservative systems in the form of amplitude-dependent modal properties. Several techniques have been proposed for this, including the Harmonic Balance [20] (HB), force appropriation [5,24], shooting methods [18,41,43], spectral sub-manifolds [50], manifold finite element techniques [41,42], etc. (see [35] for a review). More recently, Quasi-Static (QS) methods have been proposed [3,16,28] that provide a rate independent framework for NMA.

The main advantage with taking a QS approach, as opposed to other approaches, lies in computational complexity. Classically, QS implementations result in a system of non-linear algebraic equations with the number of unknowns exactly equal to the number of Degrees-of-Freedom (DoFs) of the system. On the other hand, HB implementations [21] involve an increased number of unknowns (the DoFs scaled by approximately two times the number of harmonics employed for the truncation, see Appendix A for details), and shooting method implementations [18] involve several transient solution steps for the main trajectory and the Jacobian/Monodromy matrix perturbations. The disadvantage with the HB methods is that the cost for the matrix operations grows by $\mathcal{O}\left(N_d^3 N_h^3\right)$, where N_d is the number of DoFs and N_h is the number of harmonics. When it comes to the shooting method, the main disadvantage (apart from the issues faced with transient solvers) is that the Jacobian calculation is usually conducted using finite differences with respect to each unknown since explicit analytical gradients can not always be found. By contrast, classical QS methods have no more unknowns than the number of DoFs in the discretized model and the necessary analytical Jacobians are straight forward to estimate.

The research and applied interest in QS methods, in part due to the above reasons, for modal characterization and analysis of large non-linear structures (with dissipative non-linearities, for instance) has been steadily increasing [3,6,7,13,14,17,25,27,28,48,53]. The QS method formulated in [3] referred to as *Quasi-Static Modal Analysis* (QSMA), is arguably one of the most popular among

* Corresponding author.
E-mail address: brake@rice.edu (M.R.W. Brake).

https://doi.org/10.1016/j.compstruc.2019.106184
0045-7949/© 2019 Elsevier Ltd. All rights reserved.

these presently. The method is based on modal QS properties of linear systems applied to dissipative structures under the assumption that Masing's hysteretic rules [12,30] apply in a global sense. Although normal force-coupling and applications to systems with unsymmetrical hystereses (thus violating Masing's hypotheses) are not explicitly dealt with in QSMA, recent efforts by the authors [9] have shown that these are issues that may be accommodated after making minor modifications. The major drawback with these methods is that the mode-shapes are assumed to be fixed and are not updated with response amplitude level, thereby restricting the applicability. One exception to this is an earlier work [16] that provides computational algorithms for updating mode shapes by splitting the domain into locally non-linear (jointed, for instance) and linear parts. However, the formal definition of the mode shapes as that of a nonlinear mode is still not very clear.

The current paper presents the formulation and applications of a novel QS technique for the NMA of non-linear dynamical structural systems. The method is presented as a generalization of the principle of stationarity of Rayleigh quotients from linear vibration theory (finding first application in Rayleigh's iterative methods [39]). The formulation defines non-linear modes in a manner that is analogous to the solution of a linear eigenvalue problem, whereby it is demonstrated that this analogy degenerates to equivalence when the considered system is linear. The proposed method is intended to capture amplitude-dependent characteristics of mode shapes as well as modal frequencies. It does this by extending the concept of Rayleigh quotients to both non-linear conservative as well as non-conservative systems (such as those with hysteretic dissipative elements). Further, the provided formulation accounts for static forces in a coupled fashion, thereby establishing a "finite perturbation" interpretation (akin to infinitesimal perturbation employed for linearization) for the non-linear modes. The main focus of the current investigation is dissipative dynamical systems. Therefore, applications to systems with contact non-linearities in the form of concentrated/distributed unilateral springs and/or elastic dry friction elements will be its apotheosis. Nonetheless, a simple 2-DoF conservative non-linear system is considered briefly for completeness.

The rest of the paper is organized as follows: Section 2 introduces the formalism of the Rayleigh quotient stationarity approach while drawing parallels with linear vibration theory and other QS approaches; Section 3 provides some details pertinent for problems with hysteretic elements; Section 4 provides three example applications to demonstrate the applicability of the method along with comparisons to CQSMA (a coupled QSMA formulation) and HB methods; and Section 5 provides key discussions and conclusions the authors draw from the paper. Since the paper is only concerned with the formulation of the QS method, the frequency-domain methods employed for comparison are not described in great detail. Short presentations are, however, provided in the Appendices for reference.

2. Formulation

The current section provides the formulation of the proposed Non-linear Modal Analysis (NMA) approach. Consider a discrete Multi-Degree-Of-Freedom (MDOF) *static problem* (that may be non-linear as well as non-conservative) of the form

$$\begin{aligned} &\mathbf{K}\underset{\sim}{u}+\underset{\sim}{f}_{nl}\left(\underset{\sim}{u};\underset{\sim}{u}_0\right)=\underset{\sim}{f}_s, \\ &\text{with,}\quad \underset{\sim}{u},\underset{\sim}{u}_0,\underset{\sim}{f}_s\in\mathbb{R}^n;\quad \mathbf{K}\in\mathbb{R}^{n\times n}; \\ &\qquad \underset{\sim}{f}_{nl}:\mathbb{R}^n\times\mathbb{R}^n\to\mathbb{R}^n \end{aligned} \tag{1}$$

where $\mathbf{K}$ denotes the stiffness matrix of the linear portion; $\underset{\sim}{u}$ denotes the displacement vector; $\underset{\sim}{f}_{nl}\left(\underset{\sim}{u};\underset{\sim}{u}_0\right)$ denotes the non-linear forcing that could have a history dependence in the form of $\underset{\sim}{u}_0$; and $\underset{\sim}{f}_s$ represents an external static forcing. The principle of virtual work (quoted verbatim from Reddy [40]) states that *a continuous body is in equilibrium if and only if the virtual work of all forces, internal and external, acting on the body is zero in a virtual displacement:*

$$\delta\mathcal{W}=0. \tag{2}$$

Applied to the system in Eq. (1) this becomes,

$$\delta\underbrace{\left[\int_{\underset{\sim}{u}_{ref}}^{\underset{\sim}{u}}\left\langle\mathbf{K}\underset{\sim}{x}+\underset{\sim}{f}_{nl}\left(\underset{\sim}{x};\underset{\sim}{u}_0\right)-\underset{\sim}{f}_s,d\underset{\sim}{x}\right\rangle\right]}_{\mathcal{W}}=0, \tag{3}$$

$$\text{with the inner product}\left\langle\underset{\sim}{a},\underset{\sim}{b}\right\rangle:=\sum_{i=1}^{n}a_ib_i\quad\text{for}\ \underset{\sim}{a},\underset{\sim}{b}\in\mathbb{R}^n. \tag{4}$$

Here, $\underset{\sim}{u}_{ref}$ is some fixed reference configuration used for defining the total work done. This may also be interpreted as an optimization problem of the integral term inside the square brackets with respect to $\underset{\sim}{u}$, for which Eq. (1) gives the first order optimality conditions.

There exist various interpretations of Rayleigh's quotient in the context of vibration problems (e.g., [34,38,40]). Here, the Rayleigh's quotient (occurring as the Lagrange multiplier of optimization) will be interpreted using the results of the *Courant-Fischer theorem* [34]:

> *The Rayleigh quotient for an MDoF discrete vibration problem λ is the Lagrange multiplier required for the optimization of the potential energy integral of a static problem constrained by orthonormality conditions weighted by the mass matrix ($\mathbf{M}\in\mathbb{R}^{n\times n}$).*

The corresponding solution (DoF vector) is interpreted as the dynamic mode of the underlying system. Mathematically, this is given as

$$\begin{aligned} &\min_{\underset{\sim}{u}}\quad \mathcal{W} \\ &\text{subject to}\quad h\left(\underset{\sim}{u}\right)=\tfrac{1}{2}\left\langle\underset{\sim}{u},\mathbf{M}\underset{\sim}{u}\right\rangle-\tfrac{1}{2}q^2=0. \end{aligned} \tag{5}$$

For a linear system defined with $\underset{\sim}{f}_{nl}$ set to zero, $\underset{\sim}{f}_s$ set to zero (without loss of generality for the linear system), and symmetry and positive semi-definiteness assumed for $\mathbf{K}$, the optimization may be carried out analytically, leading to the linear programming problem:

$$\begin{aligned} \mathcal{L}&=\mathcal{W}-\lambda h\left(\underset{\sim}{u}\right) \\ &=\frac{1}{2}\left\langle\underset{\sim}{u},\mathbf{K}\underset{\sim}{u}\right\rangle-\lambda\frac{1}{2}\left\langle\underset{\sim}{u},\mathbf{M}\underset{\sim}{u}\right\rangle,\qquad (\textit{Lagrangian}) \end{aligned} \tag{6}$$

$$\Rightarrow\left.\begin{aligned}&(\mathbf{K}-\lambda\mathbf{M})\underset{\sim}{u}=0\\ &\left\langle\underset{\sim}{u},\mathbf{M}\underset{\sim}{u}\right\rangle-q^2=0\end{aligned}\right\}\left(\begin{matrix}\textit{First order}\\ \textit{Optimality conditions}\end{matrix}\right). \tag{7}$$

The first order optimality conditions Eq. (7) is the linear eigenvalue problem: the solution $\underset{\sim}{u}$ is the eigenvector with mass-normalization amplitude q, and Lagrange multiplier (referred to as quotient henceforth) λ is the eigenvalue (written as ω^2 in linear dynamics problems). Note that each eigen-pair $\left(\lambda,\underset{\sim}{u}\right)$ is a local minimum with

the Lagrangian being locally quadratic (see [38], for instance, for proofs).

Although the *Courant-Fischer theorem* provides further properties for extracting arbitrary eigen-pairs for linear systems by enforcing orthonormality conditions of the solution with lower eigenvectors, only the local quadratic property will be employed in the current work. This is due to orthonormality across modes not being established for non-linear systems. On the other hand, there have been some studies that have established results similar to the quadratic minimum property even for dissipative systems [36], which motivates the generalization of the above procedure for the non-linear problem arising out of its static work done ($\mathcal{W}$ in Eq. (3)), whose constrained local minima are defined as the non-linear dynamic mode eigen-pairs.

The static forcing $\underset{\sim}{f}_s$ presents an additional consideration that has to be taken into account before defining the optimality conditions for the non-linear case. In classical vibration analyses of structures with static loads, dynamic modes are defined based on the linear system yielded by the linearization of the system about the static equilibrium and interpreted in the sense of an infinitesimal perturbation. Using this same idea, the orthogonality constraint in Eq. (5) is rewritten in terms of finite deviations of the solution $\underset{\sim}{u}$ about the static solution $\underset{\sim}{u}_s$ (which solves the *static problem* in Eq. (1) exactly) as

$$\frac{1}{2}\left\langle \left(\underset{\sim}{u}-\underset{\sim}{u}_s\right), \mathbf{M}\left(\underset{\sim}{u}-\underset{\sim}{u}_s\right)\right\rangle - \frac{1}{2}q^2 = 0. \tag{8}$$

After replacing the constraint in Eq. (5) by this, the first order optimality conditions for the problem becomes,

$$\mathbf{K}\underset{\sim}{u} + \underset{\sim}{f}_{nl}\left(\underset{\sim}{u};\underset{\sim}{u}_0\right) - \lambda\mathbf{M}\left(\underset{\sim}{u}-\underset{\sim}{u}_s\right) - \underset{\sim}{f}_s = 0 \tag{9a}$$

$$\left\langle \left(\underset{\sim}{u}-\underset{\sim}{u}_s\right), \mathbf{M}\left(\underset{\sim}{u}-\underset{\sim}{u}_s\right)\right\rangle - q^2 = 0. \tag{9b}$$

From a numerical perspective, this presents a set of $n+1$ equations (n equilibrium equations and one mass normalization condition) with $n+1$ unknowns (n-variate DoF vector $\underset{\sim}{u}$, and the quotient λ). The system size is thus one more than that of classical QS problems. The square-root of the quotient provides the natural frequency numerically for each response amplitude q. Furthermore, the formalism allows for the definition of a non-linear mode as *a non-trivial finite perturbation about the static solution that is locally stationary in the total work done.* These modes ($\left(\underset{\sim}{u}-\underset{\sim}{u}_s\right)/q$) will be referred to as Rayleigh-Quotient-based Non-linear Modes (RQNMs), and the procedure itself will be referred to as RQNM Analysis (RQNMA) in the remainder of the paper. This definition of non-linear modes is in contrast with previous definitions that are based on periodic solutions [19,52], but is potentially congruent with invariant manifold-based definitions [45,46,50].

It must be noted that the first condition (Eq. (9a)) is similar to the equation solved both in [16] as well as in the simplified QSMA [28]. The major difference here is that no attempts are made to express the solution or the dynamic forcing term as multiples of the "modal" displacement or acceleration vectors. Where the previous methods drive the simulation using mass-normalized modal forcing amplitudes, the algebraic system (Eq. (9)) is driven by the mass-normalized modal displacement amplitudes directly. Despite Eq. (9a) not appearing to contain a dissipative term, damping is introduced by the irreversibility in the non-linear forcing $\underset{\sim}{f}_{nl}$. The equation, therefore, must not be interpreted as denoting an undamped non-linear system.

2.1. Implementations with dissipative components

Following the generic formulation of RQNMA in Section 2, the next step is to focus on its extension to non-conservative systems in more detail. The following subsections (and Section 3 to some extent) expand on the consideration of linear proportional damping and arbitrary hysteretic damping terms in the framework.

2.1.1. Incorporation of linear proportional damping

First, the incorporation of linear proportional damping is considered. Since the current formulation is derived only for real modes, only damping matrices that are proportional to the mass matrix may be used for accurate solutions. Strictly speaking, stiffness proportionality must be avoided since linearization at different modal amplitudes will yield different stiffness matrices and the damping is no longer decoupled for all amplitude levels. When the static problem has solution $\underset{\sim}{u}_s$, and the optimization problem (Eq. (9)) has solution pairs $\left(\lambda(q), \underset{\sim}{u}(q)\right)$ (functions of amplitude q), the non-linear modal properties are estimated as

$$\textit{Natural frequency}: \quad \omega_n(q) = \sqrt{\lambda(q)}; \tag{10a}$$

$$\textit{Mode shape}: \quad \phi(q) = \frac{1}{q}\left(\underset{\sim}{u}-\underset{\sim}{u}_s\right); \qquad \text{and} \tag{10b}$$

$$\textit{Linear Viscous damping factor}: \quad \zeta_n(q) = \frac{\langle \phi(q), \mathbf{C}\phi(q)\rangle}{2\omega_n(q)}. \tag{10c}$$

Note that all of these are functions of mass normalized amplitudes q, which indicates the level of response.

2.1.2. Incorporation of hysteretic damping

For more general systems with dissipative non-linearities, the dissipative elements, when expressed as hysteretic terms, can be incorporated into the formulation as described here. Implementation of these require either explicit rate-dependence or the use of previous states of the element (such as displacements and forces) [9,12,31]. Fig. 1 depicts, in four steps, the different parts of hysteretic characterization necessary for the current QS formulation. Initializing the hysteretic non-linearities with zero previous states, the system is solved for a set of modal displacement amplitudes q making small increments using continuation (step 1). The state of the hysteretic elements at the end of this, denoted by P_0, is used to re-initialize the hysteretic terms. This is followed by unloading to the negative displacement amplitude (step 2). Resetting the hysteretic elements once again with the state here (M_0) and loading the system once again completes the characterization procedure for one particular amplitude level ($|q|$ at points P_0 and M_0).

A crucial aspect to note here is that the unloading and reloading curves pass through $q = 0$. At these points, the constraint in Eq. (9b) implies that the solution has to be $\underset{\sim}{u} = \underset{\sim}{u}_s$ (since $\mathbf{M}$ is taken to be positive definite). This cancels out the λ-quotient term in the first optimality condition, making Eq. (9a) the same as the *static problem*, but with the hysteretic elements updated with a different previous point (P_0 as opposed to O in Fig. 1). This could, in general, yield a solution that is different from $\underset{\sim}{u}_s$, rendering the system unsolvable. For small values of $|q|$ around zero, however, the quotient λ may have to grow arbitrarily large in order to balance out the additional forces due to a different initial setting for the hysteretic terms. Due to this, classical numerical continuation techniques [4] (such as the arc-length method) may not be usable. Classical continuation methods work by having a tangent-predictor and a constrained corrector to continue along the solution curve. Therefore, the solution point will asymptotically

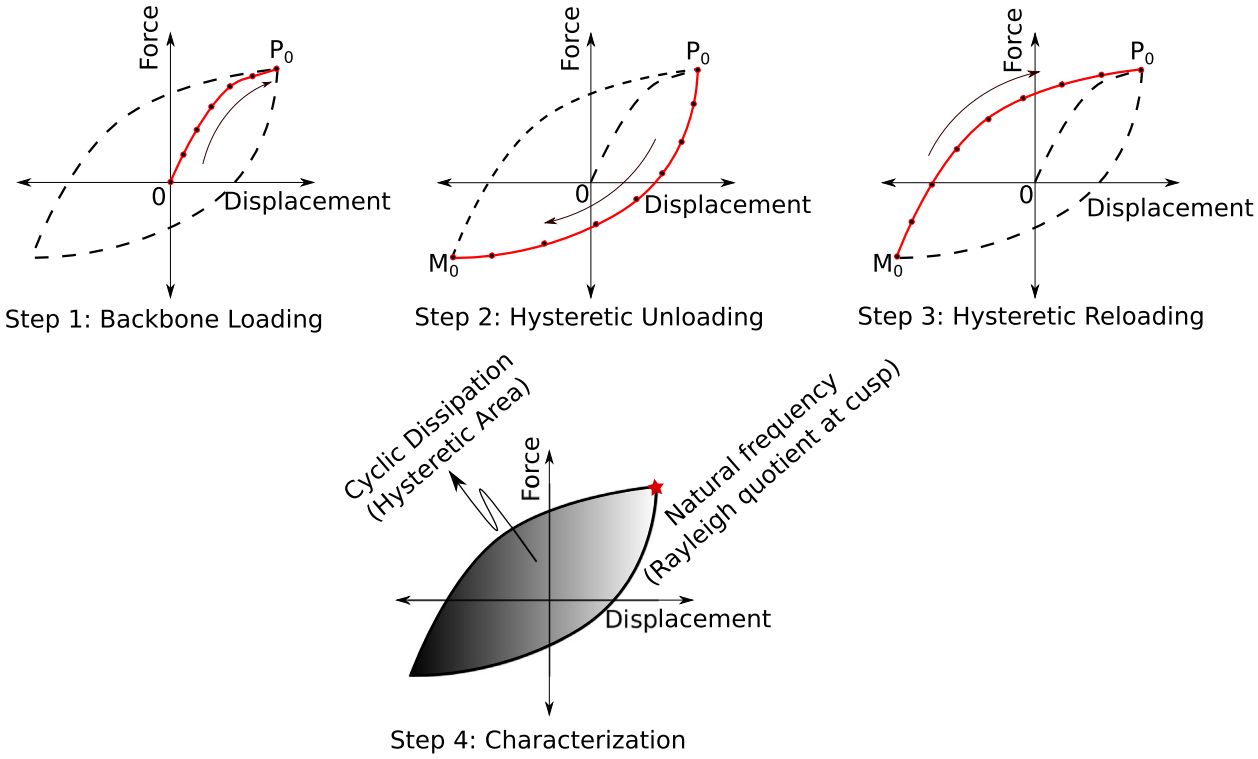

Fig. 1. Schematic representation of quasi-static characterization for hysteretic systems.

approach $q = 0$ without a possibility of stepping over it since the slope with respect to at least one of the unknowns (the quotient λ) becomes unbounded here. Since these issues are not present for sequential/natural parameter continuation (where there is no concept of predictors and correctors and the parameter q only needs to be incremented monotonically), this has been followed (for the most part) in the current study to avoid such issues. Moreover, the physical meaning of the quotients on the hysteresis loop is not readily apparent. Nonetheless, the quotients will be presented graphically in Section 4 for some observations and discussions. This issue is a moot point, though, if the hysteretic models employed all obey Masing's rules exactly, in which case the backbone loading alone (step 1 in Fig. 1) is sufficient to obtain all hysteretic properties (numerical continuation may be employed here).

The amplitude-dependent natural frequency and mode-shape of a particular load level are defined as those calculated at the corresponding locations on the backbone (using the formulae in Eq. (10)), while the damping factor is calculated based on the sum of areas under the respective hystereses of the different elements in the system (as in previous studies [9,28]). Specifically, once the hysteretic area is obtained and denoted by $D(q)$, the equivalent modal linear viscous damping factor is calculated using the formula

$$\zeta(q) = \frac{D(q)}{2\pi(\omega_n(q)q)^2}. \tag{11}$$

Since linear dissipation is unavoidable at low amplitudes, an estimate is made based on the **C** matrix (as in Section 2.1.1) and added to this to get the total equivalent modal linear viscous damping factor

$$\zeta_{eff}(q) = \frac{D(q)}{2\pi(\omega_n(q)q)^2} + \frac{\langle \phi(q), \mathbf{C}\phi(q)\rangle}{2\omega_n(q)}, \tag{12}$$

which is a combination of the damping factor based on the hysteretic non-linearities in Eq. (11) and the linear viscous contribution in Eq. (10c).

3. Details on hysteretic modeling

Hysteretic non-linearities are different from state-dependent non-linearities in that hysteretic terms need to be modeled with respect to a reference point (or state). There are several models that employ explicit rate-dependent relationships to define the evolution of the non-linearity using a first order differential equation of the form

$$\dot{f_h} = f(u, \dot{u}, \ldots; \theta), \tag{13}$$

where $u, \dot{u}$ have been used to denote a displacement-like variable and its time derivatives; θ has been used to denote constant parameters for the model; and $f()$ denotes some functional relationship (see Mathis et al. [31] for a survey of such models). Adding a differential evolution for hysteretic terms in a system is problematic in two ways: (1) exact implementation would involve additional degrees-of-freedom that increases the problem size and thus computational complexity; and (2) it is inconvenient for QS formulations, which are inherently rate independent. For the above two reasons, there have been several regularization methods applied to such models in time and frequency domains (as noted in [22]).

The hysteretic model that will be used for all of the examples in the current paper will be the elastic-dry friction element, which has an evolution given by

$$\dot{f_h} = \begin{cases} k_t \dot{u} & |f_h| \leqslant f_{slip} \\ 0 & otherwise \end{cases}. \tag{14}$$

Here, f_{slip} is the slip limit, taken to be a coefficient of friction μ multiplied by the normal force f_N. For the frequency domain (reference) simulations, the time-discretized formulations in Siewert et al. [47] (for single tangential coordinates) and Afzal et al. [1] (for two tangential coordinates) are employed. For the QS simulations, the finite difference procedure (also employed in [9]) with respect to a reference state defined by displacements u_0 and forces f_0 is employed. In a two-dimensional setting (single tangential coordinate), the friction force may be expressed as,

$$f_h = \begin{cases} k_t(u-u_0)+f_0 & |k_t(u-u_0)+f_0| \leqslant f_{slip} \\ f_{slip} & otherwise \end{cases}. \tag{15}$$

These parameters (u_0, f_0) define a state on the hysteretic curve, and need to be saved for carrying out the procedure outlined in Fig. 1.

3.1. Distributed non-linearities

For certain applications (such as the one in Section 4.3), it becomes necessary to define friction over a region (defined by a set of elements in a finite element setting). Here, phenomenological hysteretic models may be employed in the traction-displacement level rather than the classical force-displacement level [23]. This would require an additional integration step for computing the actual non-linear forces in the system. Since finite elements will be used for the most part in this paper, numerical integration using quadrature points (at interior Gauss-Legendre points) is conducted. For some implementational details, the interested reader is referred to Balaji et al. [9] where this was used in a Zero-Thicknesss-Element (ZTE) framework [32] for a more involved hysteretic model.

The hysteretic modeling formulation described here and the dissipative characterization procedure outlined in Section 2.1.2 makes this particularly useful for problems with unsymmetrical hystereses and/or intermittent hysteretic components, thereby not obeying Masing's rules. Since most commonly encountered applications, such as bolted joints, turbine blades, etc., have elements violating Masing's rules, the proposed method is very advantageous. Furthermore, the approach naturally lends itself to general non-linear hysteretic problems such as plasticity where the concept of non-linear modal analysis potentially has significant practical utility.

4. Application examples

The current section applies and compares the developed QS method RQNMA with a fixed mode-shape static-coupled QS formulation (reminiscent, but not identical to QSMA; see [9] for the formulation) referred to as CQSMA and the frequency-domain technique known as the Extended Periodic Motion Concept [20] (EPMC). After a brief study on a conservative system, two examples with different types of contact-based non-linearities are studied in detail.

4.1. System with cubic stiffness

Although the primary focus of the current paper is on hysteretic dissipation, the method itself has broader applicability. To demonstrate this, the first example is a 2-DoF oscillator with a cubic spring (studied analytically first in [46]). Numerically, the system has been extensively studied previously in [19]. The governing differential equations for the autonomous system are

$$\begin{bmatrix} 1 & 0 \\ 0 & 1 \end{bmatrix} \begin{Bmatrix} \ddot{x_1} \\ \ddot{x_2} \end{Bmatrix} + \begin{bmatrix} 2 & -1 \\ -1 & 2 \end{bmatrix} \begin{Bmatrix} x_1 \\ x_2 \end{Bmatrix} + \begin{Bmatrix} 0.5x_1^3 \\ 0 \end{Bmatrix} = \begin{Bmatrix} 0 \\ 0 \end{Bmatrix}. \tag{16}$$

Since this is a conservative system, hysteretic calculations are not conducted. Instead, the eigen-pairs are continued numerically on the backbone. Frequency-Energy Plots (FEPs) are obtained for the two non-linear modes calculated using RQNMA and QSMA, and compared with the results from EPMC as reference (implemented in the frequency domain with the first seven harmonics). QSMA is implemented by assuming that the mode shape is invariant with respect to amplitude, as found in linear vibration theory. Here the mode shapes are obtained by linearizing the system about the trivial configuration $(x_1 = 0, x_2 = 0)$,

$$\underset{\sim}{\phi}_1 = \frac{1}{\sqrt{2}} \begin{Bmatrix} 1 \\ 1 \end{Bmatrix} \quad \text{and} \quad \underset{\sim}{\phi}_2 = \frac{1}{\sqrt{2}} \begin{Bmatrix} 1 \\ -1 \end{Bmatrix}. \tag{17}$$

For RQNMA on the other hand, these mode-shapes are updated at each modal amplitude, thereby allowing one to study the amplitude-modal dependence in terms of the mode-shapes in addition to the eigenvalue characteristics.

The kinetic energy for the QS approaches may be obtained after assuming that the identified modes lead to responses $\Re\left\{\underset{\sim}{u}\, e^{i\omega_n t}\right\}$. This gives velocity amplitudes $\omega_n \underset{\sim}{u}$ that can be used to estimate kinetic energy as,

$$E_{kin} = \frac{1}{2}\left\langle \underset{\sim}{u}, \mathbf{M}\, \underset{\sim}{u} \right\rangle \omega_n^2 = \frac{1}{2} q^2 \lambda. \tag{18}$$

Here, ω_n and λ $(= \omega_n^2)$ are used to denote the eigen frequency and Rayleigh quotient respectively.

Fig. 2 is the FEP obtained for the system. It can be observed that the RQNM follows the trend of the reference closely for mode 1 but there is a relatively large offset for large amplitudes of mode 2. In those amplitude ranges, however, the system is known to demonstrate odd order internal resonances (3:1, 5:1, 7:1, etc.) leading to mode-coupling behavior. The RQNM, however, are not formulated to capture mode-coupling effects and this is thought to be the main reason behind the offset. Taking inspiration from previous studies [22,35], this region is zoomed in and presented in Fig. 2b, where certain structures on the mode 1 backbone from the EPMC solution are completely missed by RQNMA.

QSMA, on the other hand, performs poorly since the mode shape changes by a large amount in the current example and the approach is not formulated for such cases. Fig. 3 illustrates the rather large changes in the mode-shapes for the two modes. The configuration-space is planar ($\mathbb{R}^2$ space) where the mode shape may be represented as a point on a unit circle (unit magnitude, arbitrary orientation) as in Fig. 3a. It can be seen that the two modes start out perpendicular to each other (with orientations 45° and -45° respectively) for low energy conditions (which correspond to the eigenvectors of the linear part of Eq. (16)) and shifts by $+45^\circ$ asymptotically as the energy becomes larger. This trend in the orientation may be more clearly observed in Fig. 3b which plots the orientation

$$\theta = \tan^{-1}\left(\frac{x_2}{x_1}\right) \tag{19}$$

against the energy. It must be noted here that RQNMA with nearly identical computational complexity as QSMA, is able to provide solutions that represent the non-linear modes significantly better (see Section 5 for more discussions on computational effort).

4.2. Beam with frictional contact

The second example is a fixed-free Euler-Bernoulli (EB) beam FE model with a frictional element at the node corresponding to the free end that is in a uniform gravitational field in the axial direction. The beam is discretized using seven elements that are C^1 for transverse displacement DoFs and C^0 for axial displacement DoFs. Dynamic excitation is provided in the transverse direction on the penultimate node apart from the static body force due to gravity acting in the axial direction. Fig. 4 depicts a schematic representation of the model. All the physical parameters used for the model are provided in Table 1. Linear proportional damping is introduced through the Rayleigh coefficients (α, β), which are used to define the proportional damping matrix ($\mathbf{C}$) in terms of the mass and stiffness matrices ($\mathbf{M}, \mathbf{K}$ respectively) as

$$\mathbf{C} = \alpha\mathbf{M} + \beta\mathbf{K}. \tag{20}$$

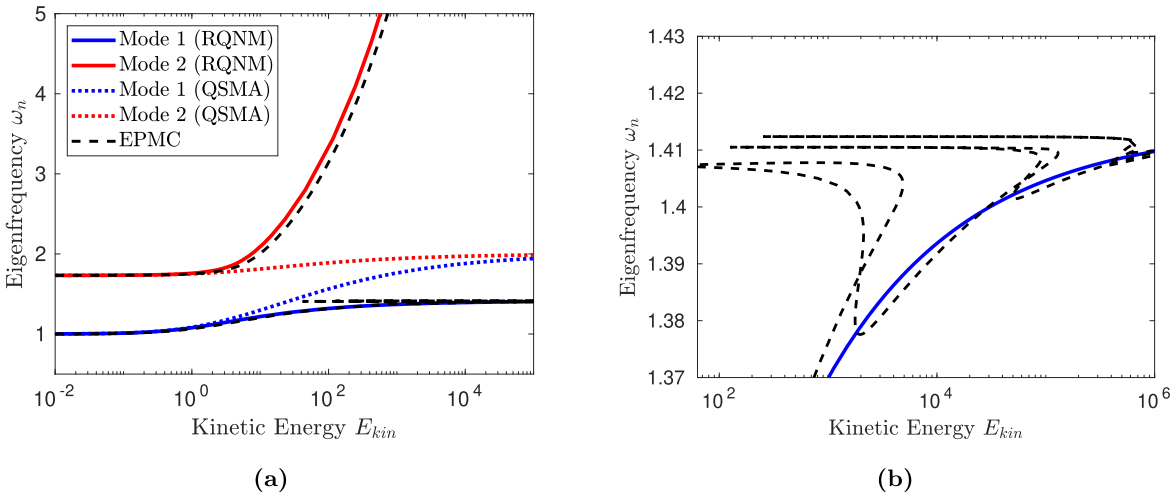

Fig. 2. Frequency-energy plot of system with cubic stiffness: (a) overview; and (b) zoomed in view of regime with modal interaction. Also plotted as reference are the results from EPMC.

This is incorporated into RQNMA through the procedure outlined in Section 2.1.1.

For generating frequency responses, the penultimate node (forcing node) is used for the response amplitude calculation. However, no forcing except for the static gravitational forcing is applied for the modal analyses. No additional prestress is applied on the contact element implying that the gravity vector must be retained in a coupled fashion throughout the analysis in order to have the contact element contribute to the response.

Since the original formulation of QSMA [28] does not account for static forces, the Coupled QSMA (CQSMA) procedure developed in Balaji et al. [9], which is also a fixed mode-shape approach, is used for comparison. The reference solution is calculated via EPMC [20], with the 0, 1, 3, 5, and 7 harmonics retained for the harmonic balance. Fig. 5 plots the frequency response of the system around the first and second resonances along with the nonlinear mode backbones. The response amplitude used here is the Root-Mean-Squared (RMS) integral amplitude of the forcing node. Note that the frequency response curves are generated in an inhomogeneous setting with dynamic forcing but the modal backbones are generated independent of forcing location, driven only by the response amplitude constraint (Eq. (9b)). It may be observed that although there are minor deviations between EPMC and the current approach (RQNM), the essential trend is captured.

Fig. 6 shows the modal backbone curves plotted for the two modes using EPMC, CQSMA and RQNM. For mode 1 (Fig. 6a–b) it can be seen that both the methods line up against the reference EPMC results equally well on the frequency plot. On the damping factor plot however, a large offset is observed in the large amplitude regime (sometimes referred to as the "fully slipped regime") where the fixed mode-shape implementation under-predicts the modal damping by about a factor of two.

The mismatch is even more pronounced for mode 2 (Fig. 6c–d), where the fixed mode-shape implementation diverges from the reference starting at the stick-slip transition phase. This results in a 5–6 Hz offset in the large amplitude region. The mismatch in

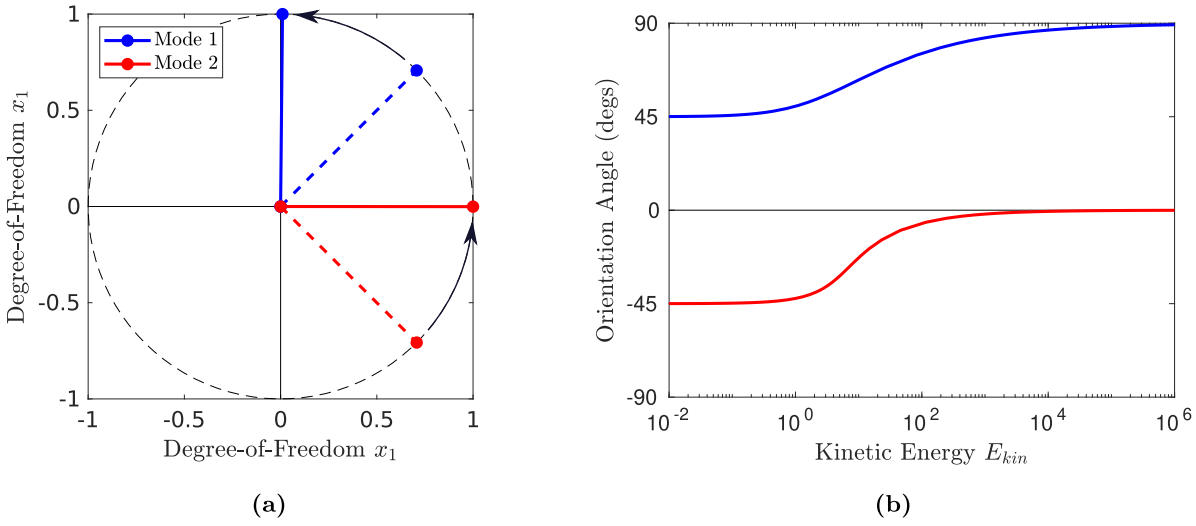

Fig. 3. Visualization of the change in mode-shape for the system in Eq. (16). Blue and red colors are used to depict the first and second modes respectively. (a) plots the initial (low energy, dashed lines) and final (high energy, solid lines) mode-shapes with arrows denoting the trends for increasing energy, and (b) plots the modal orientation angles ($\tan^{-1}(x_2/x_1)$) as a function of the kinetic energy for each mode. (For interpretation of the references to colour in this figure legend, the reader is referred to the web version of this article.)

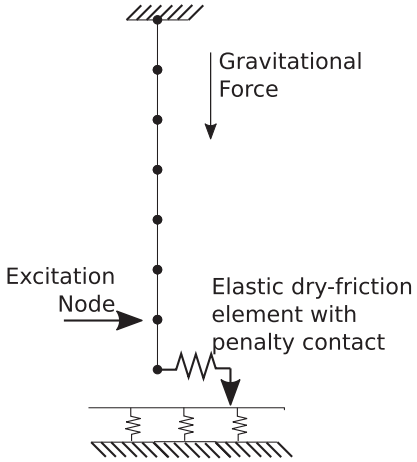

Fig. 4. Fixed-free beam with frictional element in the free end.

Table 1
Parameters used for the frictional fixed-free beam example.

Parameter	Value
Beam model	
Density	7800 kg m^{-3}
Young's modulus	200 GPa
Section area	$\pi \times 10^{-4}$ m^2
Second moment of section area	$\pi/4 \times 10^{-8}$ m^4
Total length	1 m
Gravitational acceleration	9.81 m s^{-2}
Proportional Damping (α, β)	$(0.1, 10^{-5})$
Contact element	
Coefficient of friction	0.5
Normal stiffness	10^6 N m^{-1}
Tangential stiffness	10^4 N m^{-1}

the predicted damping happens largely near the stick-slip transition region, where the true damping factor is missed by a factor of about two. Since the transition region is where most operational conditions lie, this must be taken as an indication that fixed mode-shape implementations are not reliable as the primary tool for predictive modeling. Moreover the mismatch seems to be different for different modes indicating that the applicability must be assessed on a case-by-case basis. The RQNM implementation on the other hand seems to predict the reference values near-exactly for both of the cases.

Fig. 7 illustrates the mode shape deviations as the modal amplitude q is increased. It can be seen from Fig.7a and c that the changes in mode-shape is globally nearly imperceptible. The deviation of the mass-weighted Modal Assurance Criterion [15], calculated for the i^{th} mode ϕ_i via

$$\mathrm{MAC}_{ij} = \left\langle \underset{\sim}{\phi_i}, \mathbf{M}\, \underset{\sim}{\phi_j} \right\rangle^2, \tag{21}$$

is employed for developing a quantitative understanding of the change in mode-shape. Plotted in Fig. 7b and d are the deviations of the metric from unity $(1 - \mathrm{MAC}_{ij})$. The deviation from the low amplitude mode shape saturates at about 3×10^{-3} in the large amplitude regime (and vise-versa for the large amplitude mode-shape), indicating that the frictional (operational) limits strongly influence this metric.

4.3. Bolted joint

For the third example, an idealized Finite-Element Model of the Brake-Reuß Beam (BRB) benchmark [6,10,11] is developed. In what follows, the modeling decisions are guided by insights from a higher fidelity model of the same system [6,9]. Single dimensional Euler-Bernoulli (EB) beam elements [1] are used in 3D space (C^1 elements for y and z displacements and C^0 elements for x displacements). The half-beams are constructed using separate linear EB beam models and constrained together using the contact model. Further, since the original structure contains three bolts (separated by 30 mm) in the lap joint region, the bolt-nut-washer assembly is idealized and added between appropriate nodes as C^0 bar elements in the bolt-axis directions and C^1 beam elements in the interface-planar directions. In the bolt-axis direction in addition to this, additional member stiffness is added using the relationship from [54],

$$\frac{k_{member}}{E d_{washer}} = A e^{B(d_{washer}/L_{bolt})} \Rightarrow k_{member} = 1.2041 \times 10^9 \text{ N m}^{-1}. \tag{22}$$

Here, $A_{bolt}, L_{bolt}, d_{washer}$ and E are taken as the mean cross-sectional area of the bolt, pre-stressed length of the bolt, washer outer diameter, and Young's modulus respectively. Constants A and B are taken from [54] developed for steel assemblies.

Fig. 8 shows a graphical depiction of the details of this model. The interface is discretized using eight beam elements and the rest of the (half) beam with 20 beam elements (to maintain an approximately uniform mesh size). In the assembled configuration the model has a total of (28×2) 56 elements and $((28 + 1) \times 2)$ 58 nodes with 5 DoFs each $(u_x, u_y, \theta_y, u_z, \theta_z)$. The bolt prestress is modeled using a normal traction profile that is idealized as a sum of three Gaussians centered around the bolt locations on the interface (30 mm, 60 mm, 90 mm respectively from the interface edge). The standard deviation is taken as one-sixth the pressure frustum of a washer with diameter 14.3 mm projected onto the interface with frustum angle 33°. The normal traction is thus given as

$$p_N = \frac{1}{\sigma\sqrt{2\pi}} \sum_{i=1}^{3} e^{(x-\mu_i)/\sigma^2}. \tag{23}$$

Here the μ_i's and σ denote the bolt-locations and distribution standard deviation respectively. This is then numerically integrated and scaled up by the prestress forcing to get the consistent nodal static forcing vector. A graphical representation may be seen as an inset (inset (C)) in Fig. 8. Equivalent magnitude and oppositely oriented force vectors are used for both the half beams in order to emulate the pre-stressed assembly.

Ten Gauss-Legendre quadrature points are chosen in each interfacial element for applying the non-linear contact model at the traction level (resulting in a Zero-Thickness Element formulation similar to the ones used in [9,32]). Table 2 gives the numerical values for all of the model parameters used in the subsequent analyses. The normal stiffness for the contact model k_n is fixed using the relationship from [33],

$$k_n = \frac{4P}{A\sigma\chi\sqrt{\pi}}. \tag{24}$$

The constants P, A, σ, and χ are the prestress force (11580 N), interface area (3.048×10^{-3} m^2), surface asperity peak height variance (1 μm), and Mindlin parameter (2.0) respectively [2] (comes out to be 4.287×10^{12} Pa m^{-1}).

The first bending mode in the z and y directions are studied in the coming sections. The first mode is along the bolt-axis direction and the second is along the interface-tangential direction. All HB

[1] The model is depicted in Fig. 8, where the rectangular element sections are drawn to aid visualization.

[2] Numerical values assigned guided by insight from previous work conducted by the authors.

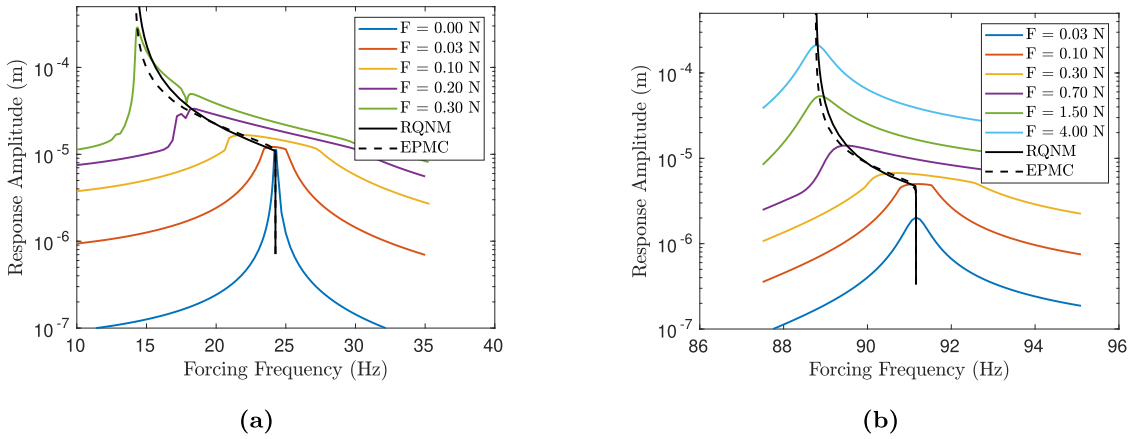

Fig. 5. Frequency Responses of the frictional fixed-free beam structure around (a) mode 1, and (b) mode 2. Also plotted are the amplitude-frequency backbones from the current procedure (RQNM, black continuous lines) and an implementation of the reference Extended Periodic Motion Concept (EPMC, black dashed lines).

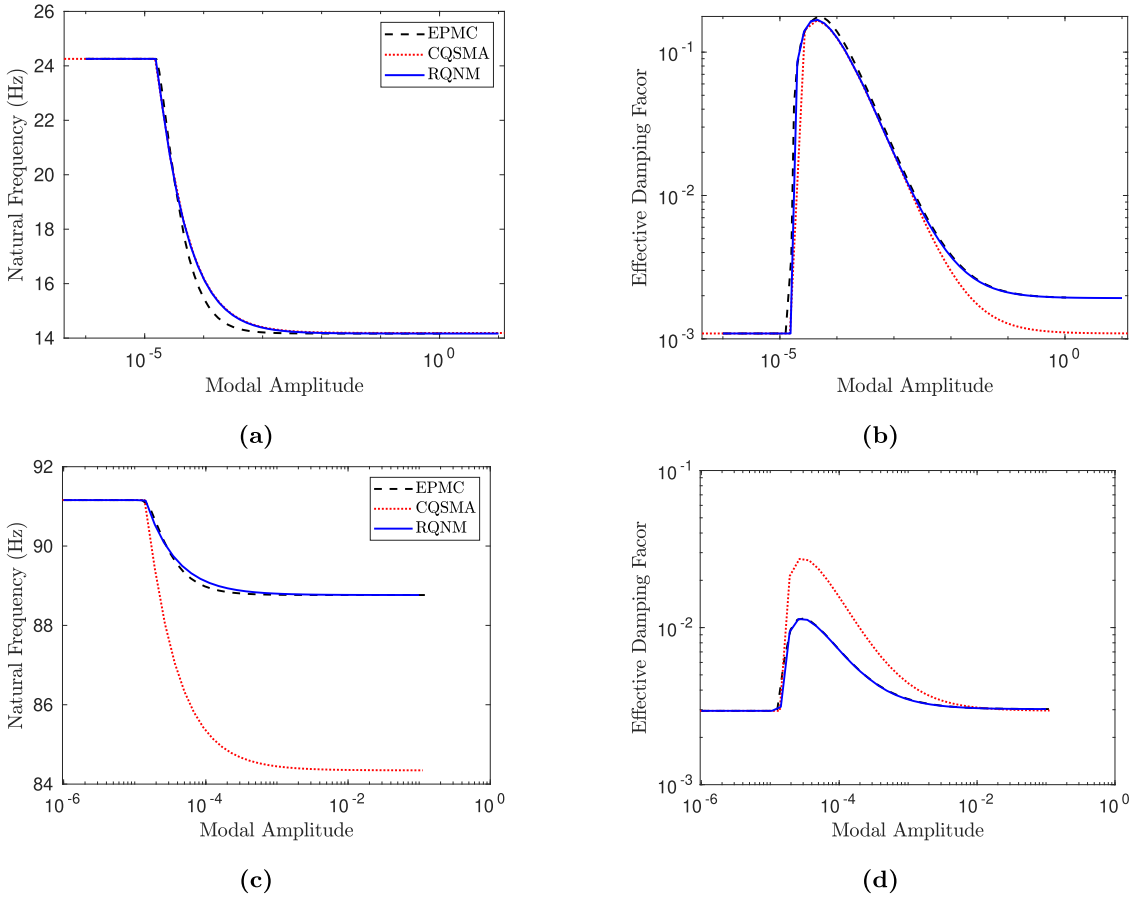

Fig. 6. Comparison with fixed mode shape implementation: (a)–(b) and (c)–(d) are modal frequency and damping characteristics for modes 1 and 2 respectively.

studies were conducted using harmonics 0, 1, 3, and 5. The even harmonics (2 and 4) were removed from the analysis since they did not contribute significantly to the responses. Rayleigh-proportional damping has been applied to the systems so that the two modes studied will have damping factor $\zeta = 10^{-3}$ at low amplitudes.

4.3.1. Bending mode 1

The EPMC analysis of this model results in a system of equations that is ill-conditioned, rendering the system numerically intractable. The authors were unable to precondition the system sufficiently well to obtain convergence over the non-linear regime. Nevertheless, a HB implementation of force-appropriation was car-

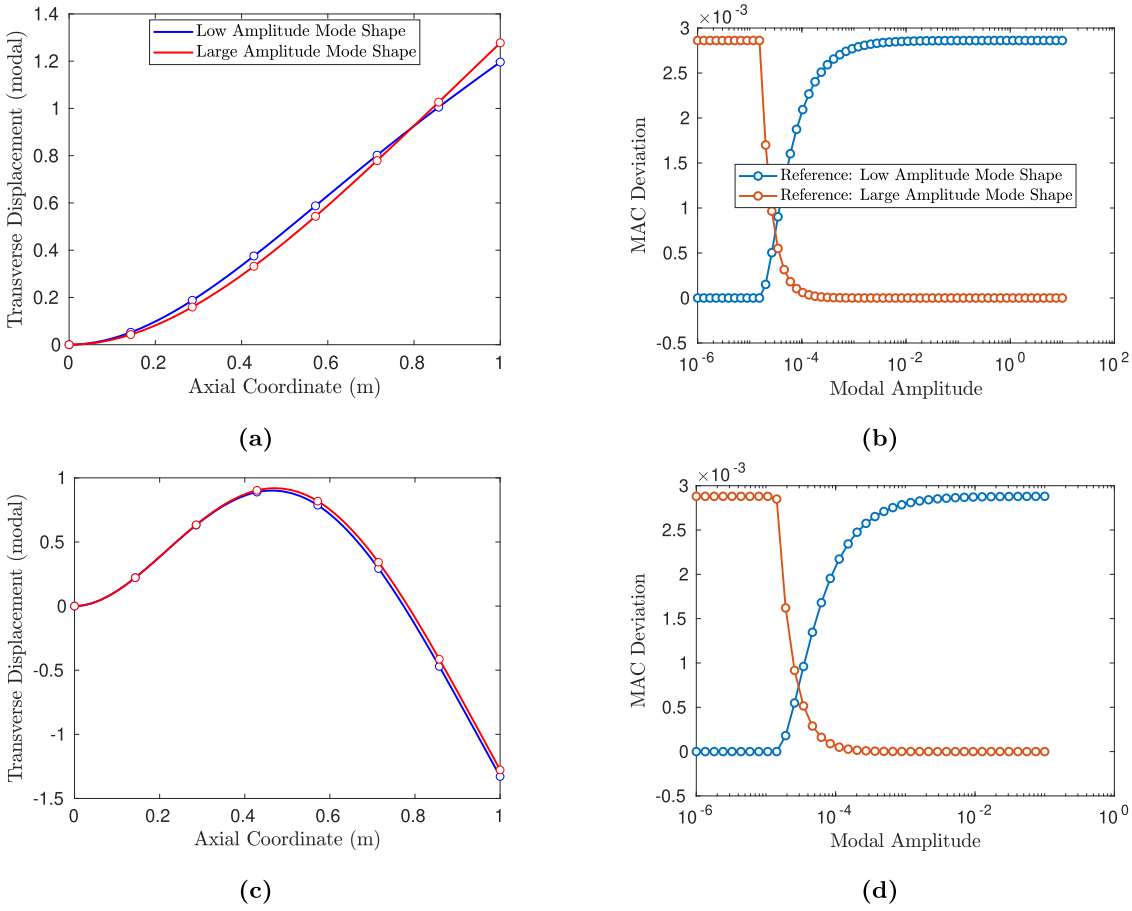

Fig. 7. Evolution of mode shapes: (a),(c) show the mode shapes at low and large amplitude regimes for modes 1 and 2 respectively; (b),(d) show the deviations of the Modal Assurance Criterion (mass-weighted, auto) for different amplitude levels for the modes 1, 2.

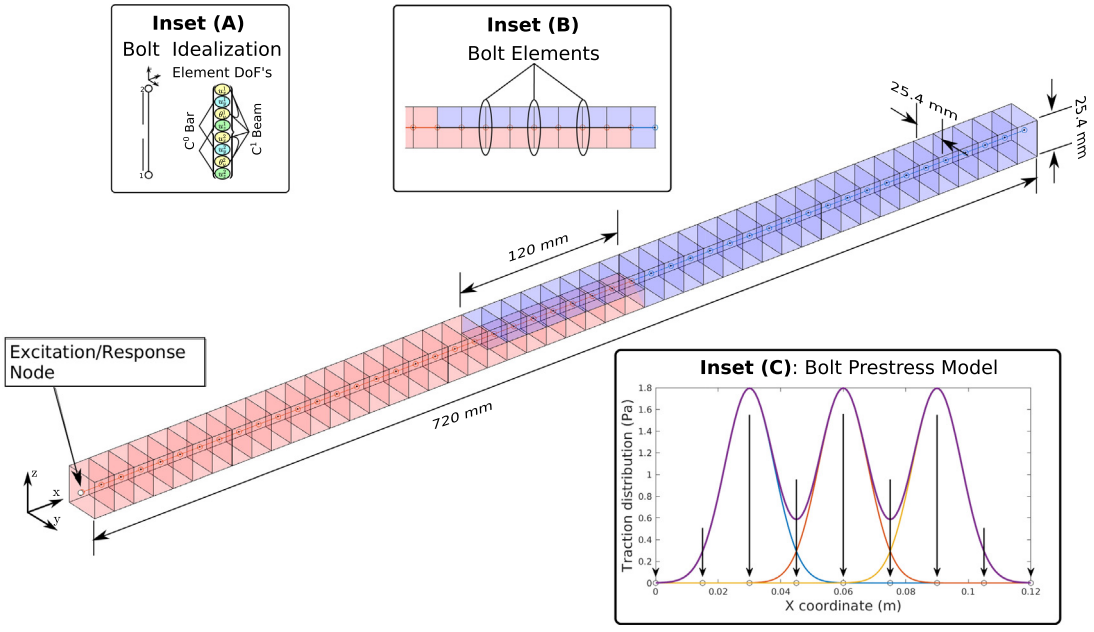

Fig. 8. Idealized Finite Element Model of the Brake-Reuß Beam (BRB). For visualization purposes, the elements have been represented as boxed using the element-sections (instead of just lines) in translucent blue and red colors to denote the different half-beams. Insets (A), (B), and (C) show details on bolt idealization, bolt elements, and prestress modeling respectively. (For interpretation of the references to colour in this figure legend, the reader is referred to the web version of this article.)

Table 2
Parameters used for the bolted joint example.

Parameter	Value
Beam elements	
Density	7857.8 kg m^{-3}
Young's modulus	192.86 GPa
Prestress (each bolt)	11580 N
Bolt-washers-nut mass	28.64 g
Bolt section diameter	6.325 mm
Contact elements	
Coefficient of friction μ	0.05
Tangential stiffnesses k_{tx}, k_{ty}	10^{10} Pa m^{-1}
Normal stiffness k_n	4.287×10^{12} Pa m^{-1}

ried out, which involved the addition of a phase constraint between the forcing and displacement at the end node (see Fig. 8).

Fig. 9 shows the results for the first bending mode. Fig. 9a shows the mode shape at different modal amplitudes, showing, that the mode-shape differs mostly near the non-linear interface and is nearly unchanged else-where. This is brought out more clearly in Fig. 10 where the relative normal displacement (difference between top and bottom beams) at the interface is plotted for the different modal amplitudes. Regions where these are negative and non-negative indicate separation and contact respectively. While a lot of difference is visible here, the nominal shape in Fig. 9a is near-identical.

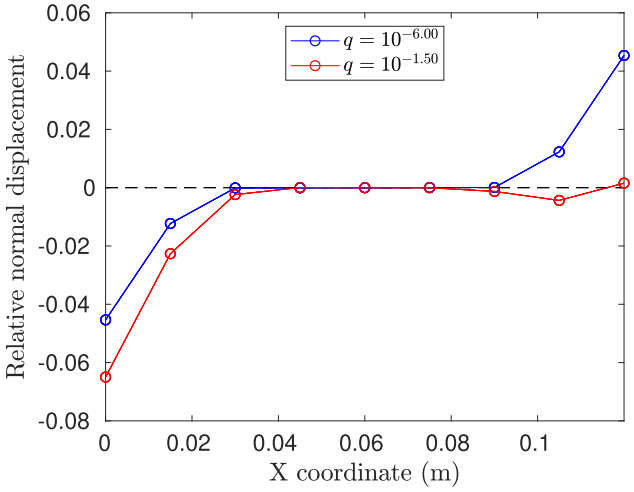

Fig. 10. Normal displacement profile for the first mode (mass normalized) extracted at two different response amplitudes.

The frequency response and backbones are shown in Fig. 9b, where it can be seen that the natural frequency predicted by the QS implementation seems to be slightly lower than the reference but the trend seems to be followed well. The same observation may be made in the modal backbones on the figure. The solution

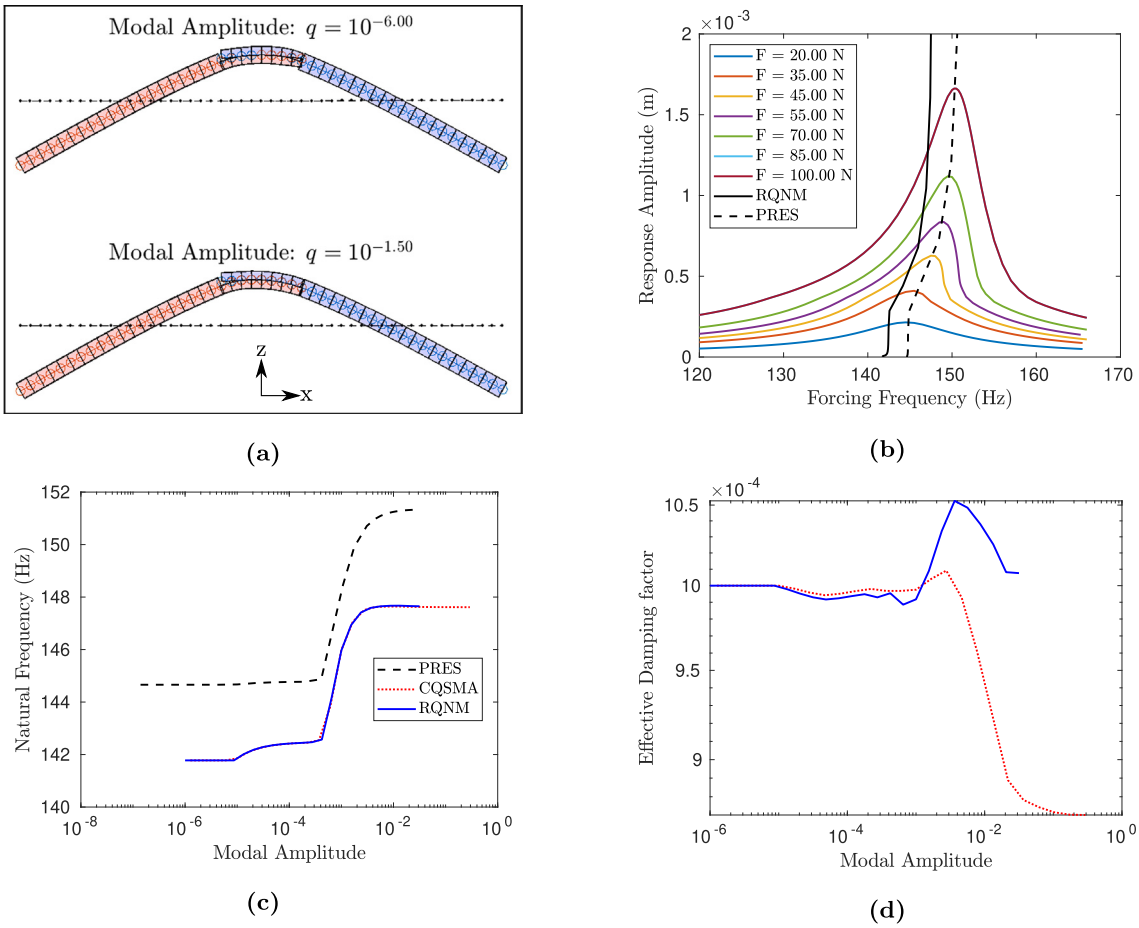

Fig. 9. Results for Bending Mode 1: (a) low and high-amplitude mode-shapes; (b) frequency response and backbones at response node - different colors indicate different forcing amplitudes and PRES refers to the Phase-Resonance reference backbone; (c)-(d) modal frequency and damping factor backbones. (For interpretation of the references to colour in this figure legend, the reader is referred to the web version of this article.)

of the phase-quadrature force appropriation is assumed to be the mode-shape and is used to estimate the modal amplitudes for plotting. Modal damping factor, on the other hand, was not estimated here since integrating the forcing and velocity over a cycle gives a measure of total dissipation and does not guarantee modal isolation. Thus, this will always be an over-prediction of the actual quantity (see Appendix A.1 for some details).

Fig. 11 shows the MAC number deviation (from Eq. (21)) to quantify the global change in mode-shape. This once again indicates a trend similar to the ones already observed in Fig. 7b (although the exercised non-linearities are different). The relatively large offset in the natural frequencies (Fig. 9b–c) is hypothesized to be due to the fact that since the response activates the unilateral contact non-linearity, it may not be possible to represent the near-resonant response using just a single mode representation. Such systems, termed "vibro-impact", have been studied extensively in the literature [2,26,29,49] and remain an active topic of research. As in Section 4.1, this is recognized as a drawback of the QS approach since it is formulated to capture just a single non-linear mode in isolation.

Fig. 12 plots the hysteretic curve (in the lower panels) and the quotients λ (relationship $\lambda = \omega^2$ employed for current studies) for different modal amplitude levels. It can be seen from the hysteresis curves that the energy dissipated due to the contact non-linearity is very little, a fact also reflected by the damping factor backbones in Fig. 9 which is nearly a straight line at around the low amplitude damping factor (10^{-3}). The quotients themselves present rather interesting trends along the hysteretic curve. As previously mentioned, around $q = 0$, the quotient decreases slightly, before increasing again. The value of the quotient at the extreme end of the cycle is used to estimate the natural frequency.

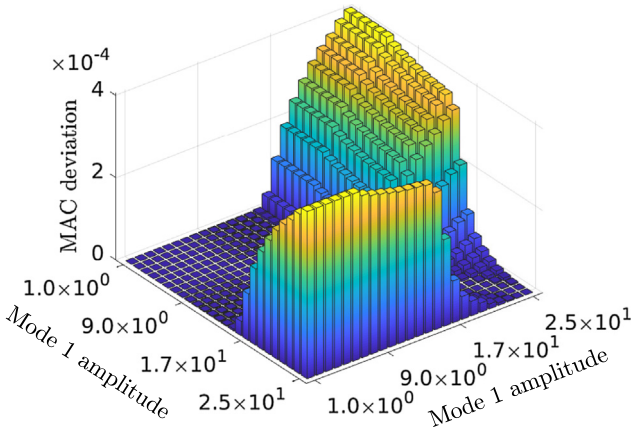

Fig. 11. Deviation in Modal Assurance Criterion: comparison of mode 1 of the beam structure in Fig. 8 estimated at different amplitudes. The planar axes are the modal amplitudes and the vertical axis indicates the MAC deviation.

4.3.2. Bending mode 2

Bending mode 2, in the interface-tangential direction, is similar to the fixed-free beam example in Section 4.2 in that frictional non-linearities, albeit in a distributed setting, are exercised here. The results of the analysis are shown in Fig. 13 in a format identical to Fig. 9.

From the mode-shapes in Fig. 13a, it can be seen that in the low amplitude (linear) regime most of the energy is stored in the elastic portions of the beam (half-beam structures), evidenced by the small gradients and relative translations in the interface region. At higher amplitudes however, the half-beams look nominally straight, while the amount of relative displacement in the interface region is rather large, showing that most of the energy here is being stored (or cyclically dissipated) through the interface. Note that the amplitudes in the figure are scaled based on mass-normalization, and are thus meant for visualization purposes only.

Due to the rather large amplitudes that were used in this example, an unrealistically large amount of softening is observed in the system, as evidenced by the peak shifting by more than 100 Hz in Fig. 13b. Since frictional non-linearity is something the current method performs well for, the modal characteristic backbones lie nearly on top of the reference, as expected. The EPMC implementation is used as the frequency-domain reference here. In the stick and slip limit cases, there seems to be some offset in the damping factors (see Fig. 13d). But it must be noted that EPMC seems to over-predict the damping factor even in the linear regime (low-amplitude RQNM agrees with the prescribed linear damping factor), indicating that the "modal" response might have other modal contributions that are not captured by the QS formulation. Note here that RQNMA provides the characteristic of the mode of interest considered in isolation and therefore does not include mode-coupling effects here.

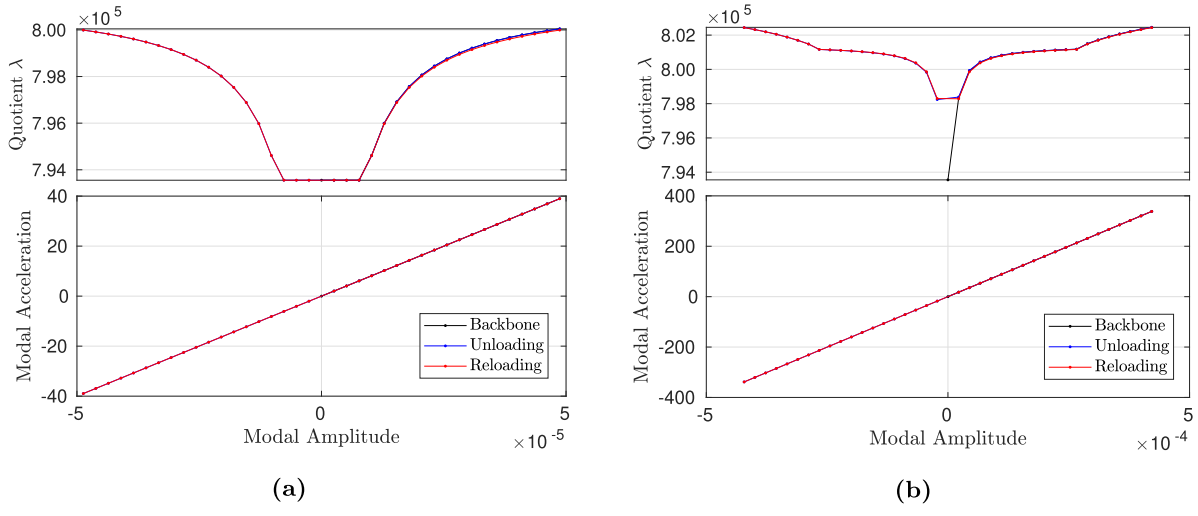

Fig. 12. The generalized Rayleigh quotients and modal hystereses plots; Each subfigure has the quotients in the top and the modal accelerations in the bottom plotted against the modal amplitude along the hysteresis loop. (a) and (b) are for low and high modal amplitude runs.

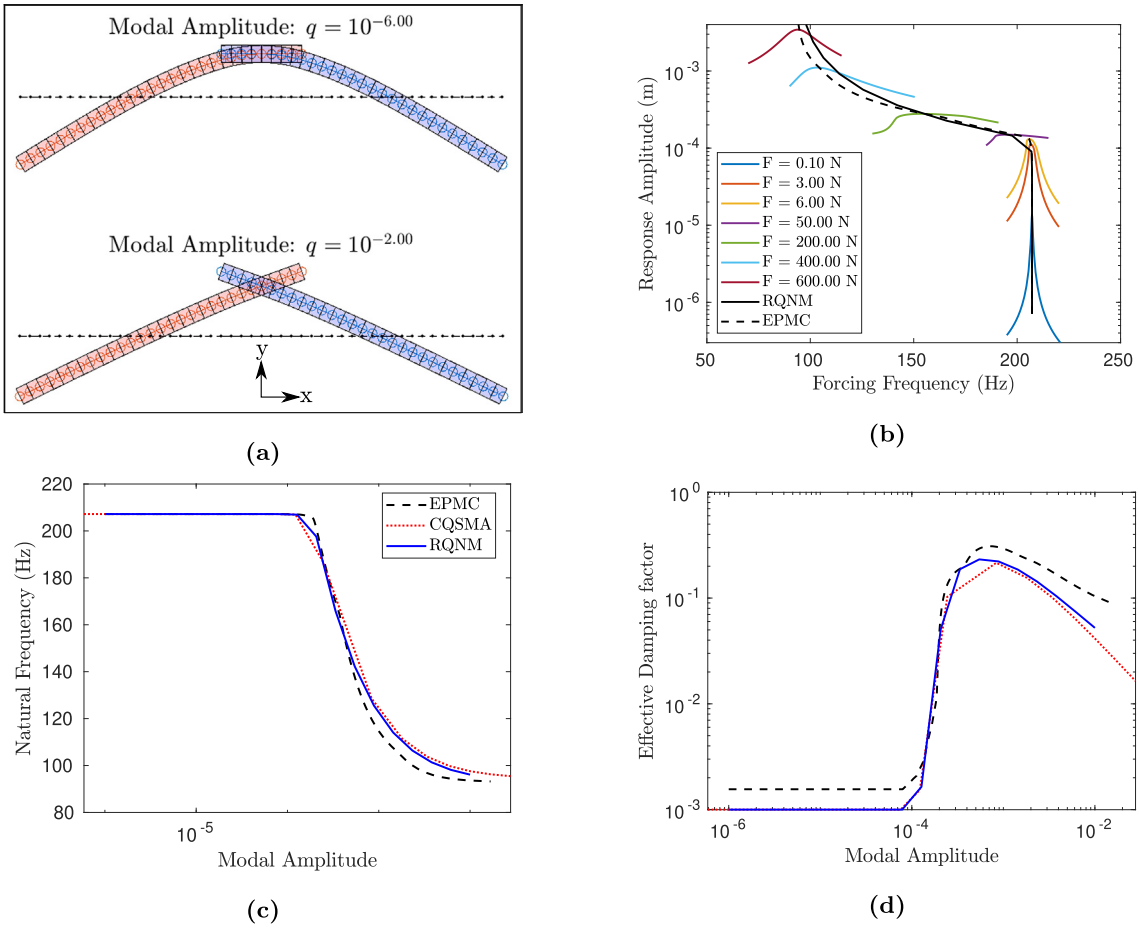

Fig. 13. Results for Bending Mode 2: (a) low and high-amplitude mode-shapes; (b) frequency response and backbones at response node; (c)-(d) modal frequency and damping factor backbones.

Once again, the deviation of the MAC number is plotted in Fig. 14 to obtain a quantitative visualization of the change of mode-shape. The magnitudes of deviation are at least two orders of magnitude larger than those seen for the first bending mode (see Fig. 11) and this is due to the fact that the mode-shapes look even globally dissimilar in this case.

Fig. 15 plots out the hysteresis paths and generalized quotients for low and high amplitude cases. The large area under the hysteresis loop for the large amplitude case reveals the strong frictional damping that is occurring. The Rayleigh quotients seem to be following a trend rather dissimilar to the one seen in Fig. 12 for the previous mode. At either side of the backbone (unloading and reloading), the quotient seems to deviate farther away from the nominal value in either direction (smaller and larger), before the trend flips at about $q = 0$. For the large amplitude case the quotient seems to even become briefly negative around $q = 0$. Increasing the number of points on the hysteresis curves reveal the same trend, indicating that these may be asymptotes tending to $\pm\infty$ as $q \to 0$ (also see earlier discussions in Section 2.1.2).

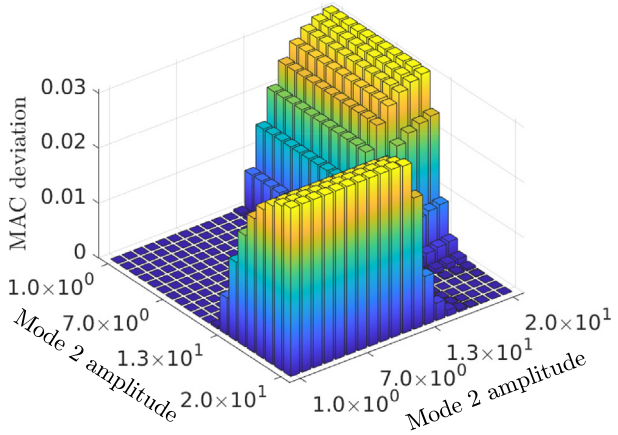

Fig. 14. Deviation in Modal Assurance Criterion: comparison of mode 2 of the beam structure in Fig. 8 estimated at different amplitudes. The planar axes are the modal amplitudes and the vertical axis indicates the MAC deviation.

In both of the above modes, the influence of assuming that the mode-shape remains fixed seems to be rather insignificant. This is however not a generic conclusion, but merely a specific observation for this particular system, since it has already been observed in the previous benchmarks (Sections 4.1 and 4.2) that fixing the mode-shape could be very misleading for certain systems from a practical standpoint.

4.3.3. Rayleigh quotients on the hysteretic curve

In order to better understand the meaning of the quotients at each point on the hysteresis curves, some closer observations for the last example are presented here. Fig. 16 plots the quotients on the backbone and the unloading and reloading curves for low and high amplitudes of the two modes under consideration. For mode 1 (Fig. 16a–b), it can be seen that the quotient on the hysteretic paths are nearly identical to those on the backbone. On the other hand, the quotients show a deviating behavior on the

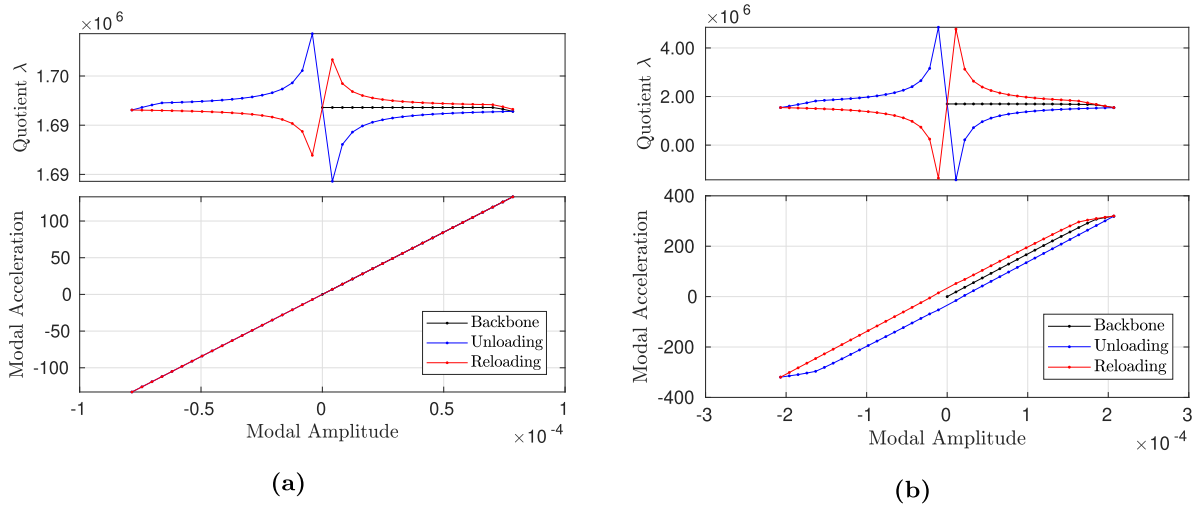

Fig. 15. The generalized Rayleigh quotients and modal hystereses plots; Each subfigure has the quotients in the top and the modal accelerations in the bottom plotted against the modal amplitude along the hysteresis loop. (a) and (b) are for low and high modal amplitude runs.

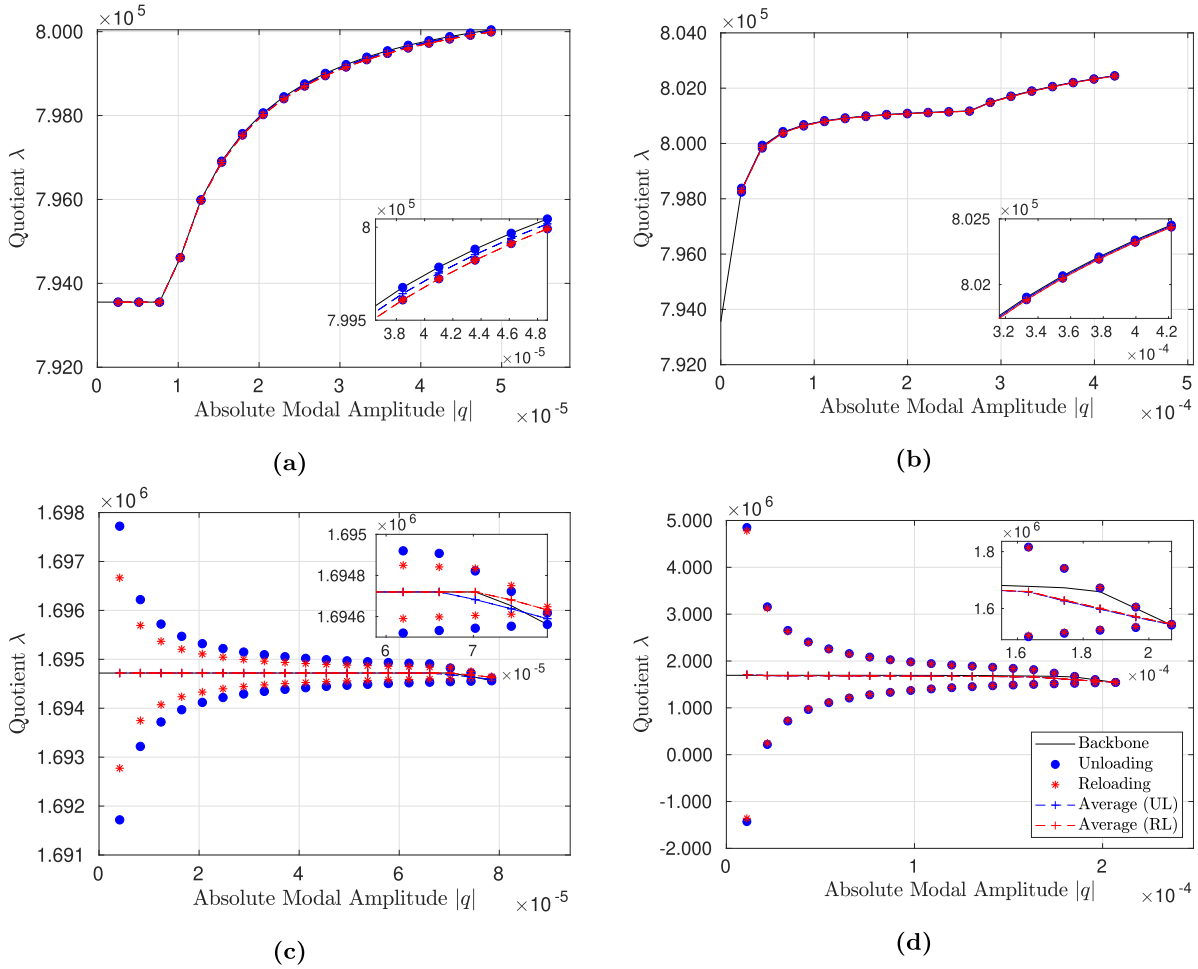

Fig. 16. Rayleigh Quotients plotted against absolute modal amplitudes for (a-b) mode 1 and (c-d) mode 2. (a),(c) and (b),(d) are low and high modal amplitudes for each case. The same amplitude levels that were used in Figs. 12–15 are used here. Average (UL) and Average (RL) are the quotients averaged over the unloading (UL) and reloading (RL) paths respectively. Insets are zoomed-in views for emphasis.

hysteretic paths for mode 2 (Figs. 16c–d). This deviation seems to grow with the maximal modal amplitude. It has already been observed, for the case in Fig. 16d, that the quotient can become negative near $|q| = 0$. It must be remarked here that hysteretic dissipation is nearly zero for mode 1 while it is the primary contribution to the damping in mode 2. For each of the plots in Fig. 16, the

averages of the quotient estimated at modal amplitudes $|q|$ and $-|q|$ (for each q) on the hysteresis curves are also plotted. The trends of these averages seem to be close, but not identical to that of the backbone. Extending the theoretical basis for the quotients in linear systems accommodates the interpretation that they are squares of the modal frequencies on the backbone curve. No similar insight with regard to the quotients on the hysteresis (or their averages) is readily apparent.

5. Discussions and conclusions

A novel Quasi-Static (QS) formulation that generalizes Rayleigh quotient stationarity for modal decomposition of linear dynamical systems to non-linear dynamical systems has been proposed and applied to benchmark problems. The formulation puts previous QS efforts at non-linear modal characterization into perspective since it may be shown that some of them may be taken as special cases of the current approach. Notably,

- by assuming that the mode-shape does not change with amplitude, the proposed Rayleigh Quotient Nonlinear Modal Analysis (RQNMA) approach reduces to the Coupled Quasi-Static Modal Analysis (CQSMA) approach in [9];
- by assuming that the mode-shape does not change with amplitude, and the hysteretic non-linearities obey Masing's rules, the RQNMA approach further reduces to the Quasi-Static Modal Analysis (QSMA) approach in [28];
- by assuming that the mode-shapes may be updated iteratively with different partitions of the domain, the RQNMA approach simplifies to the formulation in [16] in the absence of static forces.

In the context of computational costs, since the number of unknowns in a Harmonic Balance (HB) implementation is $N_d(2N_h+1)$, with N_d and N_h denoting the number of Degrees-Of-Freedom (DoFs) and harmonics respectively, the complexity of matrix inversions is $\mathcal{O}\left(N_d^3 N_h^3\right)$ (nominally), i.e., it scales with the product of the cubes of N_h and N_d. On the other hand, the number of unknowns in QS implementations is just N_d and the complexity of matrix inversions is $\mathcal{O}\left(N_d^3\right)$. For hysteretic models in each of these cases, there are sub procedures that need to be carried out: the Alternating-Frequency-Time (AFT) procedure with iterative periodic time-marching in the case of HB and Hysteretic-Marching (HM) in the case of the QS methods. The relative cost of these sub-steps must be determined on a case-by-case basis since AFT does not involve any matrix solutions (other than the FFT procedure) while HM procedures are a set of non-linear solves; the number of points in AFT are usually in the 100s, if not the 1000s, wherein non-linear function evaluations are conducted; and the number of points for HM need not be more than 50, nominally. Note that for non-hysteretic non-linearities, HM is not necessary for QS while AFT will still be necessary for HB.

Only the local minimum property of the Rayleigh quotient has been explored for the current formulation and no extensions of multi-mode orthogonality properties are pursued in the current work. A notable result for linear systems in the *Courant-Fischer theorem* is concerned with conditions for the selected eigen-pair being globally stationary for the Rayleigh quotient when it is constrained to be orthogonal to all the modes below it. Any extension of such a result to a non-linear case will have to first start with determining an appropriate orthogonalization that can be applied across multiple amplitude-dependent modes in a non-linear context.

Another possible extension of the current formulation could be the consideration of non-proportional linear damping and skew symmetric velocity proportional forces (such as models for gyroscopic effects). These are classically well known to yield complex mode-shapes and are very well understood. Although the frequency-domain techniques are known to capture these very well since the sine and cosine harmonics used there are directly related to the complex mode-shapes, there is no direct theoretical basis for QS methods to incorporate this as of writing.

Declaration of Competing Interest

None.

Acknowledgements

The authors wish to acknowledge that this paper is submitted on the 100th anniversary year of the passing of John William Strutt, 3rd Baron Rayleigh (1842-1919). Rayleigh's work has been foundational throughout the dynamics, vibrations and related communities, and the iterative procedure for modal analysis detailed in Rayleigh [39] served as the inspiration for the current work.

Funding: The authors are thankful for the support of the National Science Foundation under Grant Number 1744327.

Appendix A. Frequency-domain formulations

The current appendix provides an overview of frequency-domain Harmonic Balance (HB) formulations for Non-linear Modal Analysis (NMA). HB, as a procedure for forced response calculations, can be traced back to [51]. The idea is to transform the problem from a system of non-linear differential equations (in the time-domain) to a system of non-linear algebraic equations in the frequency domain. A truncated Fourier ansatz of the form

$$\underset{\sim}{u}(t) = \underset{\sim}{U}_0 + \sum_{k=1}^{N_h} \underset{\sim}{U}_k^c \cos(k\omega t) + \underset{\sim}{U}_k^s \sin(k\omega t) \quad \underset{\sim}{u} : \mathbb{R} \to \mathbb{R}^{N_d} \tag{25}$$

$$\text{Harmonic Coefficients} : \underset{\sim}{U}_0, \underset{\sim}{U}_k^c, \underset{\sim}{U}_k^s \in \mathbb{R}^{N_d}\,(k = 1, \ldots, N_h)$$

is applied to all quantities in the time domain after assuming that the solution $\underset{\sim}{u}(t)$ is periodic with circular frequency ω. Stacking all of the harmonic coefficients into $\underset{\sim}{U} = \left[U_0 \sim TU_1^c \sim TU_1^s \sim T\ldots\right]^T$ gives a vector of size $(N_d(2N_h+1)\times 1)$. Recasting the dynamical system in terms of $\underset{\sim}{U}$ gives

$$\underbrace{\mathbf{M}\underset{\sim}{\ddot{u}}(t) + \mathbf{C}\underset{\sim}{\dot{u}}(t) + \mathbf{K}\underset{\sim}{u}(t) + \underset{\sim}{f}_{nl}\left(\underset{\sim}{u}, \underset{\sim}{\dot{u}}, \ldots\right) = \underset{\sim}{f}_{ext}(t)}_{\text{Time domain problem}}$$

$$\Rightarrow \underbrace{\widetilde{\mathbf{E}}(\omega)\,\underset{\sim}{U} + \widetilde{\underset{\sim}{F}}_{nl}\left(\underset{\sim}{U}\right) = \widetilde{\underset{\sim}{F}}_{ext}}_{\text{Frequency domain problem}}. \tag{26}$$

Here $\widetilde{\mathbf{E}}(\omega)$ represents the so-called harmonic stiffness matrix that represents the linear part of the original system and $\widetilde{\underset{\sim}{F}}_{nl}$ is the frequency domain representation of the non-linear force $\underset{\sim}{f}_{nl}$ evaluated either through convolutions (for polynomial non-linearities) or through Alternating-Frequency-Time procedures (for more generic non-linearities). Solving this set of equations provides the non-linear steady-state periodic solution, if it exists, when the system is excited periodically at some frequency ω. Typically, frequency sweeps are conducted to obtain a more expanded picture of the response of the system. More details on the formulation and procedures involved may be found in [21].

A.1. Phase quadrature based force appropriation

The forced response of a linear system may be solved analytically and conditions derived on the relationships between the frequency, damping, and amplitude at resonance. A particularly useful property is that when the phase between the response and the forcing is exactly -90°, the corresponding frequency is ω_n, the undamped natural frequency of the linear system. Using this idea, the fundamental harmonic frequency ω in Eq. (26) may be set as an additional unknown, and the phase-lock condition yields an additional equation. In the frequency domain, this condition is given simply as $\widetilde{F}_{ext}^{T}\underset{\sim}{U}=0$. The augmented system thus becomes

$$\begin{aligned}&\widetilde{\mathbf{E}}(\omega)\underset{\sim}{U}+\widetilde{F}_{nl}\left(\underset{\sim}{U}\right)=\widetilde{F}_{ext}\\&\widetilde{F}_{ext}^{T}\underset{\sim}{U}=0.\end{aligned}\tag{27}$$

Solving Eq. (27) for $\left[\underset{\sim}{U}^{T}\omega\right]^{T}$ gives an estimate of the undamped nonlinear mode of interest. Since the procedure is closely dependent on the type of forcing applied, it is important to ensure that appropriate DoFs are excited to expose the mode of interest.

The total cyclic dissipation may be estimated using the work done by the force, calculated as

$$D=\int_{-\pi/\omega}^{\pi/\omega}\underset{\sim}{f}_{ext}(t)^{T}\,\underset{\sim}{\dot{u}}(t)dt.\tag{28}$$

This integral may be evaluated in the frequency domain directly using a result known as Parseval's theorem [21] that exploits the orthogonality of sines, cosines, and their harmonics over the principal domain of the fundamental cosine. Although this represents the total dissipation and not the modal dissipation, this is the limit of an analysis based solely on phase quadrature.

A.2. The extended periodic motion concept

A more recent method, developed in [20], is a method that is independent of the type of applied forcing. The method proposes to replace the external forcing with forcing that is more compatible with classical force appropriation (wherein forces are applied in the "shape" of the velocity vector). The external force thus becomes $f_{ext}(t)=\xi\mathbf{M}\dot{u}$ with ξ being the unknown parameter, which is interpreted as negative damping. This yields a set of $N_d(2N_h+1)$ Fourier coefficients, one fundamental frequency ω, and one parameter ξ as unknowns, totaling to $N_d(2N_h+1)+2$ unknowns. Two constraints are then added to the original system in Eq. (26) in the form of (a) a mass-normalization, giving meaning to a modal amplitude quantity; and (b) a phase-normalization, to fix the phase of the obtained complex mode (the same condition as in the previous subsection may be used). The approach is convenient in many ways, including that both the natural frequency and the damping factor (scaled by $2\omega_n$) are unknowns and are directly obtained from the simulations, and that there is great control on the numerical conditioning of the system of equations by rewriting the problem in terms of mass-normalized mode-shapes instead of the displacement vector.

In all of these approaches, the incorporation of static forces comes in just at the zero-harmonic level ($\underset{\sim}{\widetilde{F}}_{ext,0}$). The mode amplitude scaling and normalization is only applied for the non-zero harmonics and thus the static problem can "co-exist independently". This un-scaled set of DoFs (and forcing) in the system, however, presents challenges in conditioning the system of equations on a numerical implementation. This was the same reason that the authors were unable to find solutions with this method in Section 4.3.1.

References

[1] Afzal M, Lopez Arteaga I, Kari L. An analytical calculation of the Jacobian matrix for 3d friction contact model applied to turbine blade shroud contact. Comput Struct 2016; 177:204–17 [ISSN 00457949].

[2] AL-Shudeifat MA, Wierschem N, Quinn DD, Vakakis AF, Bergman LA, Spencer BF. Numerical and experimental investigation of a highly effective single-sided vibro-impact non-linear energy sink for shock mitigation. Int J Non-Linear Mech 2013;52:96–109 [ISSN 0020-7462]. <http://www.sciencedirect.com/science/article/pii/S0020746213000322>.

[3] Allen MS, Lacayo RM, Brake MRW. Quasi-static modal analysis based on implicit condensation for structures with nonlinear joints. In: International conference on noise and vibration engineering, Leuven, Belgium; September 2016.

[4] Allgower EL, Georg K. Introduction to Numerical Continuation Methods Classics in Applied Mathematics. Society for Industrial and Applied Mathematics; 2003. ISBN 9780898715446. URL https://books.google.com/books?id=LC-pmGMCGkwC.

[5] Atkins PA, Wright JR, Worden K. An extension of force appropriation to the identification of non-linear multi-degree of freedom systems. J Sound Vib 2000;237(1): 23–43 [ISSN 0022-460X]. <http://www.sciencedirect.com/science/article/pii/S0022460X00930335>.

[6] Balaji NN, Brake MRW. The surrogate system hypothesis for joint mechanics. Mech Syst Signal Process 2019;126:42–64 [ISSN 0888–3270].

[7] Balaji NN, Brake MRW. On the modal surrogacy of joint parameter estimates in bolted joints. In: Kerschen G, Brake MRW, Renson L, editors. Nonlinear structures and systems, vol. 1, p. 137–40. Springer International Publishing, Cham, 2020. ISBN 978-3-030-12390-1 978-3-030-12391-8. <http://link.springer.com/10.1007/978-3-030-12391-8_18>..

[8] Balaji NN, Chen W, Brake MRW. Traction-based multi-scale nonlinear dynamic modeling of bolted joints: Formulation, application, and trends in micro-scale interface evolution. Mech Syst Signal Process (submitted).

[9] Balaji NN, Krishna IRP, Padmanabhan C. A multi-harmonic generalized energy balance method for studying autonomous oscillations of nonlinear conservative systems. J Sound Vib 2018; 422:526–41 [ISSN 0022460X]. <http://linkinghub.elsevier.com/retrieve/pii/S0022460X1830141X>..

[10] Brake MRW, editor. The mechanics of jointed structures. Springer; 2017.

[11] Brake MRW, Schwingshackl CW, Reuß P. On the observed variability and repeatability in jointed structures. Mech Syst Signal Process 2019;129:282–307.

[12] Brake MRW. An overview of constitutive models. In: The mechanics of jointed structures. Springer; 2018. p. 207–21.

[13] Cooper SB, Rosatello M, Mathis AT, Johnson K, Brake MRW, Allen Matthew S, et al. Effect of far-field structure on joint properties. In: Dynamics of coupled structures, vol. 4, p. 63–77. Springer; 2017. <http://link.springer.com/chapter/10.1007/978-3-319-54930-9_7>.

[14] Dreher T, Balaji NN, Groß J, Brake MRW, Krack M. Gerrymandering for interfaces: Modeling the mechanics of jointed structures. In: 37th International modal analysis conference (IMAC XXXVII), Orlando, FL; January 2019.

[15] Ewins DJ. Modal testing: theory. 2nd ed. Hertfordshire: Practice and Appliaction. Research Studies Press Ltd.; 2000.

[16] Festjens H, Chevallier G, Dion J-L. A numerical tool for the design of assembled structures under dynamic loads. Int J Mech Sci 2013;75:170–7.

[17] Jewell EA, Allen MS, Lacayo R. Predicting damping of a cantilever beam with a bolted joint using quasi-static modal analysis. In: Volume 8: 29th Conference on mechanical vibration and noise, Cleveland, Ohio, USA; August 2017. p. V008T12A019 ASME. ISBN 978-0-7918-5822-6. <http://proceedings.asmedigitalcollection.asme.org/proceeding.aspx?doi=10.1115/DETC2017-67859>.

[18] Kerschen G. Computation of nonlinear normal modes through shooting and pseudo-arclength computation. In: Kerschen G, editor, Modal analysis of nonlinear mechanical systems, CISM International Centre for Mechanical Sciences. Springer Vienna, Vienna; 2014. p. 215–50 [ISBN 978-3-7091-1791-0]. doi:https://doi.org/10.1007/978-3-7091-1791-0_5.

[19] Kerschen G, Peeters M, Golinval JC, Vakakis AF. Nonlinear normal modes. part I. A useful framework for the structural dynamicist. Mech Syst Signal Process 2009;23:170–94.

[20] Krack M. Nonlinear modal analysis of nonconservative systems: extension of the periodic motion concept. Comput Struct 2015;154:59–71 [ISSN 00457949]. <http://linkinghub.elsevier.com/retrieve/pii/S0045794915000978>..

[21] Krack M, Gross J. Harmonic balance for nonlinear vibration problems. mathematical engineering. Cham: Springer International Publishing; 2019. ISBN 978-3-030-14022-9 978-3-030-14023-6. http://link.springer.com/10.1007/978-3-030-14023-6.

[22] Krack M, Panning-von Scheidt L, Wallaschek J. A method for nonlinear modal analysis and synthesis: application to harmonically forced and self-excited mechanical systems. J Sound Vib 2013;332:6798–814.

[23] Krack M, Salles L, Thouverez F. Vibration prediction of bladed disks coupled by friction joints. Arch Comput Methods Eng 2017;24(3): 589–36 [ISSN 1134–3060, 1886–1784].
[24] Kuether RJ, Allen MS. Computing nonlinear normal modes using numerical continuation and force appropriation. In ASME international design engineering technical conferences IDETC/CIE, Chicago, IL; August 2012.
[25] Kuether RJ, Najera-Flores DA. Response predictions of reduced models with whole joints Technical Report SAND2018-6002C. Albuqurque, NM: Sandia National Laboratories; 2018.
[26] Kurt M, Chen H, Lee YS, McFarland DM, Bergman LA, Vakakis AF. Nonlinear system identification of the dynamics of a vibro-impact beam: numerical results. Arch Appl Mech 2012;82:1461–79.
[27] Lacayo R, Pesaresi L, Groß J, Fochler D, Armand J, Salles L, et al. Nonlinear modeling of structures with bolted joints: a comparison of two approaches based on a time-domain and frequency-domain solver. Mech Syst Signal Process 2019; 114:413–38 [ISSN 0888–3270]. <https://www.sciencedirect.com/science/article/pii/S0888327018302875>.
[28] Lacayo RM, Allen MS. Updating structural models containing nonlinear Iwan joints using quasi-static modal analysis. Mech Syst Signal Process 2019;118:133–57 [ISSN 08883270].
[29] Lee YS, Nucera F, Vakakis AF, McFarland DM, Bergman LA. Periodic orbits, damped transitions and targeted energy transfers in oscillators with vibro-impact attachments. Phys D: Nonlinear Phenom 2009; 238(18): 1868–96 [ISSN 0167–2789]. <http://www.sciencedirect.com/science/article/pii/S0167278909001997>.
[30] Masing G. Self-stretching and hardening for brass. In: Proceedings of the second international congress for applied mechanics; 1926. p. 332–35.
[31] Mathis AT, Balaji NN, Kuether RJ, Brink AR, Brake MRW, Quinn DD. A review of damping models for structures with mechanical joints. Appl Mech Rev (submitted).
[32] Mayer M, Gaul L. Modeling of contact interfaces using segment-to-segment-elements for FE vibration analysis. In: 23rd International modal analysis conference (IMAC XXIII), Bethel, CT; 2005.
[33] Medina S, Nowell D, Dini D. Analytical and numerical models for tangential stiffness of rough elastic contacts. Tribol Lett 2013;49(1): 103–15 [ISSN 1023–8883, 1573–2711].
[34] Meyer CD. Matrix analysis and applied linear algebra. Philadelphia: Society for Industrial and Applied Mathematics; 2000. ISBN 978-0-89871-454-8.
[35] Peeters M, Viguié R, Sérandour G, Kerschen G, Golinval JC. Nonlinear normal modes, part II: toward a practical computation using numerical continuation techniques. Mech Syst Signal Process 2009;23:195–216.
[36] Phani AS, Adhikari S. Rayleigh quotient and dissipative systems. J Appl Mecha 2008;75(6): 061005–061005–6 [ISSN 0021–8936].
[37] Rand RH. A direct method for non-linear normal modes. Int J Non-Linear Mech 1974;9:363–8.
[38] Rao SS. Mechanical vibrations in SI units. Pearson Education Limited; 2017. ISBN 978-1-292-17861-5. https://books.google.com/books?id=REQ4DwAAQBAJ.
[39] Rayleigh JWSB. The theory of sound. Number v. 1 in the theory of sound. Macmillan 1877.
[40] Reddy JN. Energy principles and variational methods in applied mechanics. Wiley; 2002, ISBN 978-0-471-17985-6. https://books.google.com/books?id=3gw5rxLQdaQC.
[41] Renson L, Deliège G, Kerschen G. Finite element computation of nonlinear normal modes of nonconservative systems. In: In Proceedings of the ISMA conference 2012.
[42] Renson L, Deliége G, Kerschen G. An effective finite-element-based method for the computation of nonlinear normal modes of nonconservative systems. Meccanica 2014;49:1–16.
[43] Renson L, Kerschen G, Cochelin B. Numerical computation of nonlinear normal modes in mechanical engineering. J Sound Vibr 2016;364:177–206 [ISSN 0022460X]. <https://linkinghub.elsevier.com/retrieve/pii/S0022460X15007543>.
[44] Rosenberg RM. Normal modes of nonlinear dual-mode systems. J Appl Mech 1960;27:263–8.
[45] Shaw SW, Pierre C. Non-linear normal modes and invariant manifolds. J Sound Vib 1991;150:170–3.
[46] Shaw SW, Pierre C. Normal modes for non-linear vibratory systems. J Sound Vib 1993;164:85–124.
[47] Siewert C, Panning L, Wallaschek J, Richter C. Multiharmonic forced response analysis of a turbine blading coupled by nonlinear contact forces. J Eng Gas Turb Power 2010;132(8):082501 [ISSN 07424795].
[48] Singh A, Wall M, Allen MS, Kuether RJ. Spider configurations for models with discrete Iwan elements. In: Kerschen G, Brake MRW, Renson L, editors, Nonlinear structures and systems. Springer International Publishing, Cham 2020; 1, p. 25–38 [ISBN 978-3-030-12390-1 978-3-030-12391-8]. <http://link.springer.com/10.1007/978-3-030-12391-8_4>.
[49] Sracic MW, Allen MS, Sumali H. Identifying the modal properties of nonlinear structures using measured free response time histories from a scanning laser Doppler vibrometer. In: 30th International modal analysis conference (IMAC XXX), Jacksonville, FL; February 2012.
[50] R. Szalai, D. Ehrhardt, and G. Haller. Nonlinear model identification and spectral submanifolds for multi-degree-of-freedom mechanical vibrations. Proc Roy Soc A: Math, Phys Eng Sci 2017;473(2202):20160759 URL <https://royalsocietypublishing.org/doi/full/10.1098/rspa.2016.0t759>.
[51] Urabe M, Reiter A. Numerical computation of nonlinear forced oscillations by Galerkin's procedure. J Math Anal Appl 1966;14(1): 107–40 [ISSN 0022–247X].
[52] Vakakis AF. Nonlinear normal modes (NNMs) and their applications in vibration theory: an overview. Mech Syst Signal Process 1997;11:3–22.
[53] Wall M, Allen MS, Zare I. Predicting S4 beam joint nonlinearity using quasi-static modal analysis. In: Kerschen G, Brake MRW, Renson L, editors, Nonlinear structures and systems. Springer International Publishing, Cham 2020; Volume 1, p. 39–51. ISBN 978-3-030-12390-1 978-3-030-12391-8. <http://link.springer.com/10.1007/978-3-030-12391-8_5>.
[54] Wileman J, Choudhury M, Green I. Computation of member stiffness in bolted connections. J Mech Des 1991;113(4):432 [ISSN 10500472]. <http://MechanicalDesign.asmedigitalcollection.asme.org/article.aspx?articleid=1443117>.